ORIGINAL ARTICLE

Modeling and Simulation of Gas Kick Behavior in Deviated and Horizontal Wellbores Under Variable Pressure Conditions

Naveen Perera[1] and Dilani Fernando[2]

[1] Open University of Sri Lanka, Nawala Road, Nugegoda 11222, Sri Lanka
[2] Sabaragamuwa University of Sri Lanka, Belihuloya 70140, Sri Lanka

ABSTRACT

Gas kicks represent one of the most critical transient events in well control during drilling operations, particularly in deviated and horizontal wellbores where complex hydrodynamic and transient multiphase effects arise. As modern field development increasingly targets extended-reach and unconventional reservoirs, the interplay of variable bottom-hole and surface pressure programs with gas migration and annular hydraulics requires detailed modeling and simulation. In such wells, non-vertical orientation modifies the effective hydrostatic head, enhances segregation and slip between gas and liquid phases, and alters the response of control systems such as chokes and managed pressure drilling equipment. This work presents a comprehensive modeling and simulation framework for gas kick behavior in deviated and horizontal wellbores under variable pressure conditions, combining transient multiphase flow modeling with numerical analysis and data-driven interpretation. The model incorporates depth-dependent inclination, realistic annular geometry, compressible gas behavior, and dynamic surface pressure control laws. Transient simulations are performed for a range of kick intensities, well inclinations, and pressure schedules in order to characterize gas migration, surface response, and operational envelopes. Additionally, synthetic simulation data are used to train machine-learning models for early detection and characterization of gas kicks based on surface measurements. The study emphasizes the interaction between physical modeling and data-based interpretation and explores the sensitivities of predicted kick behavior to flow, thermodynamic, and operational parameters in deviated and horizontal wells subject to variable pressure profiles.

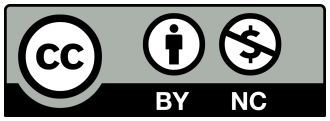

Symbol	Description	Units
s	Measured depth along the wellbore	m
z	Vertical depth (true vertical depth)	m
$\theta(s)$	Inclination angle from the vertical	rad
A	Annular cross-sectional area	m^2
D_h	Hydraulic diameter used in friction correlations	m
$\alpha_g,\ \alpha_l$	Gas and liquid volume fractions (holdups)	–
$u_g,\ u_l,\ u_m$	Gas, liquid, and mixture velocities	m/s

Table 1: Notation for basic geometric and phase-averaged flow variables in the transient wellbore model.

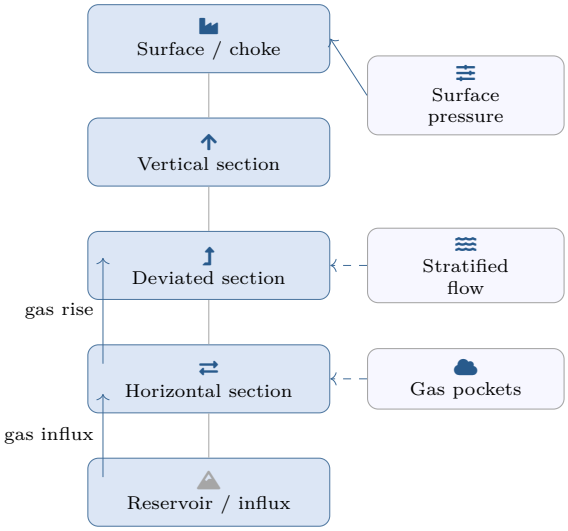

Figure 1: Schematic of the deviated and horizontal wellbore with gas influx, segregation, and surface backpressure control. The central stack represents the vertical, deviated, and horizontal sections, while side nodes emphasize stratified flow, gas pocket formation, and choke-controlled surface pressure.

1 | Introduction

Gas influx from a permeable formation into a wellbore while drilling can evolve into a gas kick when the wellbore pressure falls below the formation pore pressure [1]. If not identified and controlled in a timely manner, such events may escalate into severe well control problems. Traditional well control methods and design practices were largely developed for vertical wells, where hydrostatic and frictional contributions to the pressure profile follow relatively simple patterns. The rapid growth of deviated and horizontal drilling has significantly changed this context. Extended-reach wells, complex 3D trajectories, and tight drilling margins under managed pressure drilling strategies create conditions in which gas kick behavior is influenced by inclination-dependent hydrodynamics, elongated flow paths, and variable surface and bottom-hole pressure programs.

In deviated and horizontal wellbores, the orientation of the well relative to the gravitational field modifies the effective hydrostatic gradient, leading to spatially varying pressure support along the trajectory. Gas, being much less dense than the drilling fluid, has a strong tendency to segregate and migrate upward, but in near-horizontal segments this motion is accompanied by complex patterns of stratified or slug flow, where gas accumulates in high-side pockets and propagates as elongated bubbles or slugs [2]. This leads to transient pressure and flow signatures at the surface that differ significantly from those observed in vertical wells. At the same time, well control operations often involve active manipulation of surface pressure through choke adjustments or closed-loop managed pressure drilling systems. These operations impose time-varying boundary conditions that feed back into the multiphase flow in the annulus and may either attenuate or amplify the transient response to a

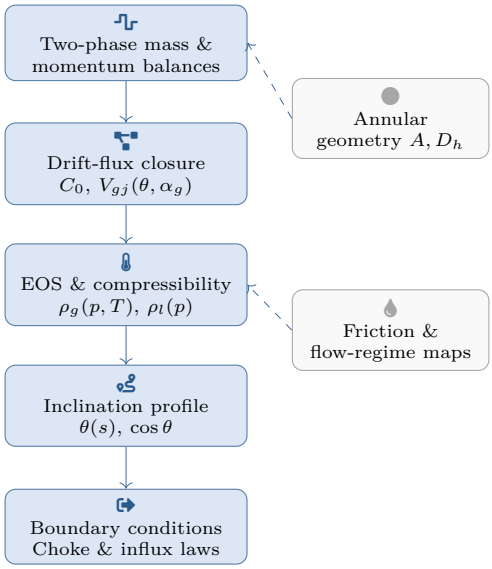

Figure 2: Structure of the transient two-phase flow model along measured depth, highlighting conservation equations, drift-flux closure, thermodynamic relations, inclination-dependent gravity, and variable boundary conditions for choke and formation influx, with annular geometry and friction correlations acting as key inputs.

gas influx.

Accurate modeling and simulation of gas kick behavior in such conditions rely on capturing the coupled dynamics of compressible gas and nearly incompressible liquid in an inclined, possibly eccentric annulus, with variable pressure constraints at the wellhead and at the downhole boundary representing the formation. Various modeling strategies can be employed, ranging from simplified single-mixture models to more detailed two-fluid or drift-flux formulations. These models are governed by systems of partial differential equations for the conservation of mass and momentum, subject to closure relations for slip velocity, phase interaction, wall friction, and thermodynamic properties. The equations are highly nonlinear and stiff due to strong couplings between pressure, phase fractions, and flow rates, especially when gas compressibility is significant and when abrupt operational changes occur at the surface [3].

In parallel with physics-based modeling, the availability of high-frequency surface measurements, including standpipe pressure, casing pressure, flow-in and flow-out rates, and pit volumes, has motivated the development of data-driven methods for detecting and classifying abnormal events. Machine-learning models trained on field data or on synthetic data from detailed simulators can provide early-warning tools for gas kicks by recognizing characteristic patterns in these time series. In deviated and horizontal wells, where transient signatures may be less intuitive than in vertical wells, such data-driven tools may be particularly valuable, provided they are informed by and consistent with the underlying physics of multiphase flow and pressure control.

This work develops an integrated framework for modeling and simulation of gas kick behavior in deviated and horizontal wellbores under variable pressure conditions, and for exploiting the resulting simulations in data-driven interpretation. A transient one-dimensional model is formulated along the well trajectory, incorporating inclination-dependent gravity, compressible gas, and dynamic boundary conditions representing surface choke control and bottom-hole influx. Numerical methods based on finite volume discretization and implicit or semi-implicit time integration are used to solve the governing equations. The resulting simulations are used to explore how well architecture, inclination, fluid properties, and pressure control strategies influence the propagation of a gas kick. Synthetic outputs are then employed to construct and evaluate machine-learning models for classification and regression tasks related to kick detection and characterization. The analysis focuses on the internal consistency of the model, the numerical robustness of the solution strategy, and the interpretability of both the physical and data-driven results with respect to operational decision making in deviated and horizontal wells.

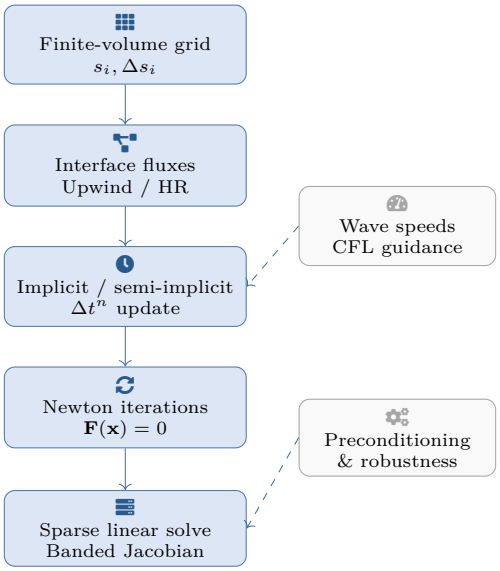

Figure 3: Numerical solution strategy based on a one-dimensional finite-volume grid, high-resolution interface fluxes, implicit or semi-implicit time stepping, Newton iterations for the nonlinear system, and sparse linear solves with stabilization and CFL analysis guiding time-step selection.

2 | Physical Background of Gas Kicks in Deviated and Horizontal Wellbores

A gas kick is initiated when the pressure in the open-hole section falls below the formation pore pressure for a sufficiently long time to allow an influx of gas or gas-bearing fluid. Under static conditions with no influx, the bottom-hole pressure is determined primarily by the hydrostatic column of the drilling fluid, with minor contributions from static friction or trapped compression. During drilling, circulation adds frictional losses that may either increase or decrease bottom-hole pressure depending on flow direction and boundary conditions. In deviated and horizontal wells, the hydrostatic contribution depends on the vertical depth rather than the measured depth, whereas frictional and inertial effects are integrated along the true length of the trajectory [4]. As a result, the same fluid density and pump rate that produce a comfortable overbalance in a vertical well may yield a reduced safety margin in a long horizontal section.
When an influx occurs, gas enters the annulus at the bottom of the well and initially mixes or disperses with the drilling fluid. As the gas experiences lower pressures while moving toward shallower depths, it expands according to its thermodynamic behavior. This expansion decreases the average density of the annular mixture and leads to a reduction of the hydrostatic head, which in turn may draw additional influx from the formation. The dynamics of this coupled process depend on the rate of gas entry, the ability of the circulating fluid to transport gas, and the time-varying pressures imposed at the surface through choke and pump operations. In vertical wells, gas rise is approximately aligned with gravity, and flow regimes may transition through bubbly, slug, churn, and annular flow patterns as gas volume fraction increases [5]. In deviated wells, and especially in long horizontal sections, gravity acts largely perpendicular to the main flow direction, creating stratification and lateral segregation that alter these regime transitions.
In inclined and horizontal annuli, gas often migrates upward preferentially along the high side of the borehole, while liquid occupies the lower side. The resulting stratification gives rise to asymmetric velocity profiles and increases the importance of interfacial shear and local turbulence. Flow may evolve into elongated gas pockets separated by liquid slugs, particularly during transient operations such as pump start-up or choke adjustments. Local accumulation of gas in near-horizontal sections may temporarily reduce surface signals of a kick, delaying its detection until the gas slug reaches a more vertical part of the well or the surface. At the same time, the expansion of these pockets with decreasing pressure can produce strong pressure surges when they are accelerated or compressed by control actions.
The pressure response at the surface during a gas kick

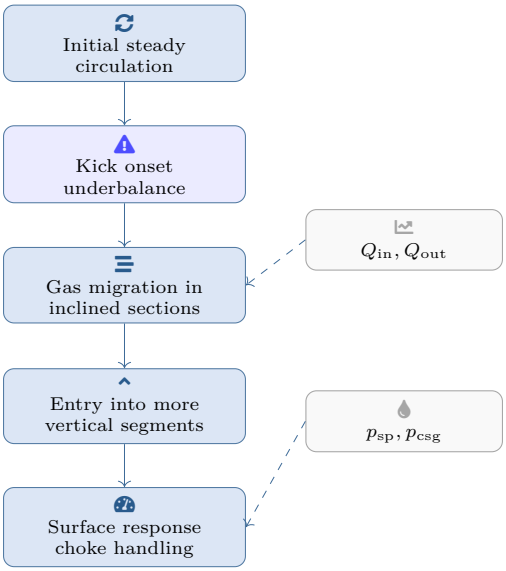

Figure 4: Representative evolution of a gas kick scenario, from steady circulation through kick onset, gas migration in deviated and horizontal sections, transition into steeper intervals, and the resulting surface signatures in flow rates and pressures during choke-controlled circulation.

in deviated or horizontal wells is shaped by the combined effect of gas migration, friction, wellbore geometry, and boundary conditions [6]. A given volume of gas influx may produce different casing pressure histories depending on whether it is trapped in a near-horizontal section, allowed to flow freely into vertical intervals, or compressed against a closed or partially opened choke. Variable surface pressure conditions, such as those arising during managed pressure drilling, further modulate the transient behavior. For example, strategies that maintain a nearly constant bottom-hole pressure through rapid choke adjustments can alter the rate at which gas migrates and expands, potentially changing the timing and magnitude of surface manifestations.

Thermodynamics and heat transfer also influence gas kick behavior. As gas migrates upward and expands, it may cool due to Joule–Thomson effects and heat exchange with the surrounding formation and drilling fluid. Temperature changes in turn affect gas density and compressibility, which feed back into the pressure and flow dynamics [7]. In most well control analyses, simplified thermal models are used, but in extended-reach horizontal wells where residence times are long and temperature gradients are significant, more detailed thermal coupling can be relevant to prediction accuracy.

Operationally, the detection and management of gas kicks in deviated and horizontal wells rely on monitoring surface measurements such as flow-in and flow-out rates, pump strokes, standpipe pressure, and pit volume, along with downhole data when available. Deviated trajectories complicate the interpretation of these measurements because signature patterns of gas influx can be spread out in time, attenuated, or masked by normal operational fluctuations. As a result, understanding the physical background of gas behavior along the wellbore trajectory, including the roles of inclination, annular geometry, and pressure control actions, is essential for building reliable models and simulations. These, in turn, can form the basis for training data-driven interpretation tools tailored to the specific challenges of non-vertical wells [8].

3 | Mathematical Formulation of Transient Two-Phase Flow

To model gas kick behavior in deviated and horizontal wellbores under variable pressure conditions, a one-dimensional description is commonly adopted along the wellbore centerline, parameterized by the measured depth coordinate denoted by s [9]. The inclination of the well relative to the vertical is described by an angle $\theta(s)$, so that the vertical depth gradient is $\mathrm{d}z/\mathrm{d}s = \cos\theta(s)$. The annular cross-sectional area is denoted by A, and an effective hydraulic diameter D_h is used in friction correlations. The flow is treated as a two-phase mixture of a liquid phase (drilling fluid) and a gas phase (influx) with

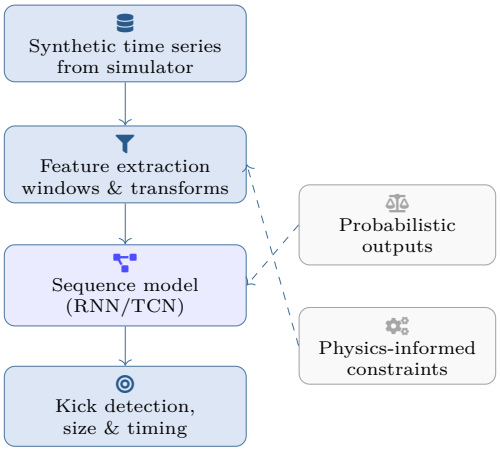

Figure 5: Data-driven interpretation layer built on synthetic time series from the simulator, where features are extracted over temporal windows and used by sequence models to infer kick-related classes and continuous quantities, with probabilistic outputs and physics-informed constraints improving robustness.

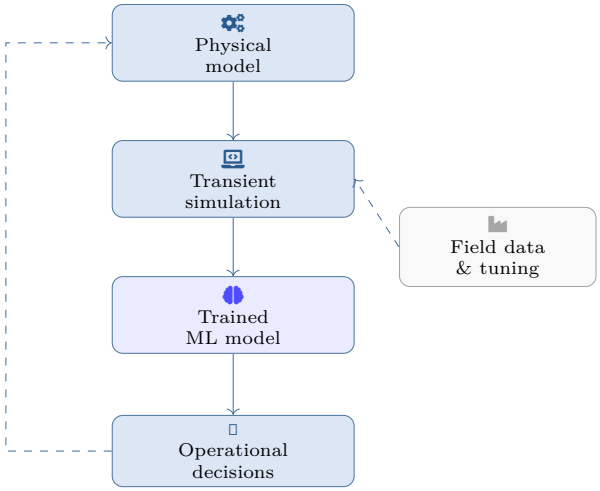

Figure 6: Integrated framework linking the physical model, transient simulator, and machine-learning layer to operational decision support, with feedback loops from field data and control actions informing model calibration and future simulations.

respective volume fractions [10] α_l and α_g, satisfying $\alpha_l + \alpha_g = 1$.

In a two-fluid formulation, separate mass conservation equations are written for gas and liquid. Denoting by ρ_g and ρ_l the densities and by [11] u_g and u_l the phase velocities, the one-dimensional mass balance for the gas phase can be expressed as

$$\frac{\partial}{\partial t}\left(\alpha_g \rho_g\right) + \frac{\partial}{\partial s}\left(\alpha_g \rho_g u_g\right) = q_g, \tag{1}$$

where q_g represents source terms such as gas influx from the formation. The corresponding equation for the liquid phase is [12]

$$\frac{\partial}{\partial t}\left(\alpha_l \rho_l\right) + \frac{\partial}{\partial s}\left(\alpha_l \rho_l u_l\right) = q_l, \tag{2}$$

with q_l capturing liquid source or sink effects, for example drilling fluid addition or losses.

Momentum conservation for each phase is described by one-dimensional momentum balance equations. For the gas phase, neglecting interfacial mass transfer and assuming that pressure is shared between phases, a typical form is

$$\frac{\partial}{\partial t}\left(\alpha_g \rho_g u_g\right) + \frac{\partial}{\partial s}\left(\alpha_g \rho_g u_g^2\right) \text{ [13]} = -\alpha_g \frac{\partial p}{\partial s} + \alpha_g \rho_g g \cos\theta - f_g, \tag{3}$$

where p is pressure, g is gravitational acceleration, and f_g is an effective friction and interfacial momentum

Relation	Expression	Comment
Gas mass	$\partial_t(\alpha_g\rho_g) + \partial_s(\alpha_g\rho_g u_g) = q_g$	Gas influx enters via q_g at the bottom cell
Liquid mass	$\partial_t(\alpha_l\rho_l) + \partial_s(\alpha_l\rho_l u_l) = q_l$	Accounts for mud sources and losses
Mixture mass	$\partial_t\rho_m + \partial_s(\rho_m u_m) = q_m$	$\rho_m = \alpha_l\rho_l + \alpha_g\rho_g$
Mixture momentum	$\partial_t(\rho_m u_m)+\partial_s(\rho_m u_m^2) = -\partial_s p+\rho_m g\cos\theta-f_m$	1D balance with gravity and friction
Gas EOS	$\rho_g = \dfrac{pM_g}{ZRT}$	Real-gas density with $Z(p,T)$
Liquid density	$\rho_l = \rho_{l0}\left[1 + c_l(p - p_0)\right]$	Slightly compressible drilling fluid

Table 2: Core governing equations used in the drift-flux based transient two-phase wellbore formulation.

exchange term that can be decomposed as

$$f_g = \tau_{gw}\frac{P_w}{A} + \tau_{gi}\frac{P_i}{A}, \tag{4}$$

with τ_{gw} and τ_{gi} representing wall and interfacial shear stresses, and P_w and [14] P_i the wetted and interfacial perimeters. A similar equation holds for the liquid phase,

$$\frac{\partial}{\partial t}\left(\alpha_l\rho_l u_l\right) + \frac{\partial}{\partial s}\left(\alpha_l\rho_l u_l^2\right) = -\alpha_l\frac{\partial p}{\partial s} + \alpha_l\rho_l g\cos\theta - f_l, \tag{5}$$

where f_l includes wall and interfacial friction acting on the liquid [15].

Direct solution of a full two-fluid model is numerically demanding and requires detailed closure relations for interfacial terms. A widely used alternative is the drift-flux formulation, which describes the mixture using a single momentum equation and introduces a relation between phase velocities. The mixture velocity u_m and mixture density ρ_m are defined by

$$u_m = \alpha_l u_l + \alpha_g u_g, \text{[16]} \tag{6}$$

$$\rho_m = \alpha_l\rho_l + \alpha_g\rho_g. \tag{7}$$

The mixture mass conservation equation then becomes

$$\frac{\partial}{\partial t}\left(\rho_m\right) + \frac{\partial}{\partial s}\left(\rho_m u_m\right) \text{[17]} = q_m, \tag{8}$$

with $q_m = q_l + q_g$. A single momentum equation for the mixture is written as

$$\frac{\partial}{\partial t}\left(\rho_m u_m\right) + \frac{\partial}{\partial s}\left(\rho_m u_m^2\right) = -\frac{\partial p}{\partial s} + \rho_m g\cos\theta - f_m, \tag{9}$$

where f_m represents an effective friction term calibrated against empirical correlations for multiphase flow in annuli [18].

The relative motion between gas and liquid is described by a drift-flux relation of the form

$$u_g = C_0 u_m + V_{gj}, \tag{10}$$

where C_0 is the distribution parameter and V_{gj} is the drift velocity. These parameters may be functions of inclination, flow regime, and gas volume fraction, and their specification is a key element of model closure. Given u_g and u_m, the liquid velocity [19] u_l is obtained from

$$u_l = \frac{u_m - \alpha_g u_g}{\alpha_l}. \tag{11}$$

Group	Definition	Interpretation
Reynolds number Re	$Re = \dfrac{\rho_m U D_h}{\mu_m}$	Inertial vs viscous forces; sets friction regime
Inverse Froude Fr^{-1}	$\mathrm{Fr}^{-1} = \dfrac{gL}{U^2}$	Relative importance of gravity and buoyancy
Pressure coefficient C_p	$C_p = \dfrac{P^\star}{\rho^\star U^2}$	Scaling of pressure to inertial effects
CFL number	$\mathrm{CFL} = \dfrac{\Delta s}{\Delta t(\lvert u_m\rvert + c_m)}$	Explicit stability constraint for wave propagation
Inclination ratio η	$\eta = \dfrac{L_{\mathrm{hor}}}{L}$	Fraction of horizontal or near-horizontal trajectory

Table 3: Dimensionless groups that govern flow regimes, inclination effects, and numerical stiffness in the simulations.

The gas density ρ_g is modeled as a compressible function of pressure and temperature. A common representation is based on a real-gas equation of state,

$$\rho_g = \frac{pM_g}{ZRT}, \tag{12}$$

where M_g is the gas molar mass, R the universal gas constant, [20] T the temperature, and Z the compressibility factor, which itself depends on p and T. The liquid is often approximated as slightly compressible, for example using

$$\rho_l[21] = \rho_{l0}\left[1 + c_l\left(p - p_0\right)\right], \tag{13}$$

where ρ_{l0} is a reference density at pressure p_0 and c_l is the liquid compressibility. When thermal effects are significant, temperature can be modeled by an energy equation coupled to the flow, but in many well control analyses a prescribed temperature profile or quasi-steady thermal model is employed.

Boundary conditions are specified at the surface [22] $s = 0$ and at the bottom $s = L$, where L is the total measured depth. At the surface, pressure is governed by choke and flow-line conditions, often represented by a relation between choke opening and flow rate. A simple algebraic model for the choke can be written as

$$p(0,t)[23] = p_{\mathrm{sep}} + \Delta p_{\mathrm{choke}}(Q_{\mathrm{out}}, u_c), \tag{14}$$

where p_{sep} is the separator pressure, Q_{out} is the flow rate leaving the well, and u_c is a control variable representing choke opening. The bottom boundary condition at $s = L$ is determined by the formation pressure and the nature of the influx. A simple influx model prescribes a gas source term

$$q_g(L,t) = \lambda\left[[24]p_f - p(L,t)\right]_+, \tag{15}$$

where p_f is the formation pressure, λ is an inflow coefficient, and $[\cdot]_+$ denotes the positive part, reflecting that gas influx occurs only when the wellbore pressure falls below formation pressure.

To analyze the dominant physical regimes and guide numerical design, it is convenient to express the

Element	Choice	Purpose
Spatial discretization	Non-uniform finite volumes along measured depth	Resolve strong gradients near surface and bottom-hole
Flux approximation	Upwind or high-resolution schemes	Stabilize transport of sharp gas fronts and slugs
Time integration	Implicit or semi-implicit scheme	Handle gas compressibility without tiny Δt
Nonlinear solver	Newton or modified Newton iterations	Robust solution of coupled mass–momentum system
Linear solver	Banded or preconditioned sparse method	Exploit 1D sparsity of the Jacobian matrix
Boundary models	Algebraic choke and influx relations	Couple wellbore hydraulics to surface and formation pressures

Table 4: Main numerical components of the finite volume discretization and solution strategy for transient kick simulation.

governing equations in dimensionless form [25]. Introducing characteristic scales for length L, velocity U, pressure $P^\star$, density $\rho^\star$, and time $T^\star = L/U$, dimensionless variables are defined, for instance,

$$\tilde{s} = \frac{s}{L}, \qquad \tilde{t} = \frac{t}{T^\star}, \tag{16}$$

$$\tilde{u}_m = \frac{u_m}{U}, \qquad \tilde{p} = \frac{p}{P^\star}, \tag{17}$$

$$\tilde{\rho}_m = \frac{\rho_m}{\rho^\star}. \tag{18}$$

Substitution into the mixture momentum equation yields [26]

$$\frac{\partial}{\partial \tilde{t}}\left(\tilde{\rho}_m \tilde{u}_m\right) + \frac{\partial}{\partial \tilde{s}}\left(\tilde{\rho}_m \tilde{u}_m^2\right) = -\frac{P^\star}{\rho^\star U^2}\frac{\partial \tilde{p}}{\partial \tilde{s}} + \frac{gL}{U^2}\tilde{\rho}_m \cos\theta - \tilde{f}_m. \tag{19}$$

The dimensionless groups $P^\star/(\rho^\star U^2)$ and gL/U^2 correspond to a pressure coefficient and an inverse Froude number, respectively. The friction term $\tilde{f}_m$ can be related to a Reynolds number defined using the mixture properties. The relative magnitude of these terms indicates whether inertial, gravitational, or frictional contributions dominate in different portions of the well.

Under variable pressure conditions, time dependence in the boundary pressures enters explicitly through the

Case	Setup	Main observation
V-ref	Vertical trajectory with nearly fixed surface backpressure	Early and clear surface signatures of influx
D-man	Deviated well with manually operated choke	Delayed signals and operator-driven pressure transients
D-MPD	Deviated well with MPD bottom-hole set-point control	Reduced influx and moderated pressure excursions
H-low	Long horizontal limb at low pump rate	Stratified gas pockets and intermittent slug motion
H-high	Long horizontal limb at high pump rate	More dispersed flow and smoother surface trends

Table 5: Representative simulated scenarios combining inclination profiles with different surface pressure control strategies.

dimensionless boundary conditions, for example [27]

$$\tilde{p}(0,\tilde{t}) = \tilde{p}_{\mathrm{surf}}(\tilde{t}), \qquad \tilde{p}(1,\tilde{t}) = \tilde{p}_{\mathrm{bh}}(\tilde{t}), \tag{20}$$

where $\tilde{p}_{\mathrm{surf}}$ and $\tilde{p}_{\mathrm{bh}}$ are prescribed or determined by control laws and formation inflow models. The resulting system of partial differential and algebraic equations describes the coupled evolution of pressure, phase fractions, and velocities along the well under the combined influence of gas influx, inclination-dependent gravity, friction, and time-varying pressure constraints.

4 | Numerical Discretization and Solution Strategy

The governing equations for transient two-phase flow are discretized using a finite volume formulation along the measured depth direction. The well is partitioned into N control volumes with cell centers at s_i and interfaces at $s_{i\pm1/2}$. Cell lengths [28] Δs_i may be non-uniform to allow local refinement near the surface or the bottom-hole region where strong gradients are expected during a gas kick. Cell-averaged quantities such as mixture density, phase volume fractions, velocity, and pressure are defined for each control volume. The conservation equations are integrated over each control volume and over a discrete time step, and spatial fluxes are approximated by numerical flux functions evaluated at the cell interfaces.
For the mixture mass conservation equation, integrating over cell i yields

$$\frac{\mathrm{d}}{\mathrm{d}t}\left([29]\rho_{m,i}A\Delta s_i\right) = F_{i-1/2} - F_{i+1/2} + Q_{m,i}, \tag{21}$$

where $F_{i\pm1/2}$ are numerical mass fluxes at the interfaces and $Q_{m,i}$ represents the integrated source term in the cell, including influx at the bottom and other volumetric terms. Mass fluxes are computed as

$$F_{i+1/2} = \hat{\rho}_{m,i+1/2}\hat{u}_{m,i+1/2}A, \tag{22}$$

where $\hat{\rho}_{m,i+1/2}$ and $\hat{u}_{m,i+1/2}$ are interface values reconstructed from neighboring cells using appropriate upwind or high-resolution schemes. In regions with strongly convective flow, an upwind-biased reconstruction is employed to maintain stability and avoid nonphysical oscillations, while preserving sharp transients in phase fraction and velocity.

The mixture momentum equation is discretized similarly. Integrating over cell i gives

$$\frac{\mathrm{d}}{\mathrm{d}t}\left([30]\rho_{m,i}u_{m,i}A\Delta s_i\right) = H_{i-1/2} - H_{i+1/2} + S_i, \quad (23)$$

where $H_{i\pm1/2}$ are numerical momentum fluxes and S_i contains source contributions from pressure gradients, gravity, and friction. The fluxes are approximated by

$$H_{i+1/2} = \hat{\rho}_{m,i+1/2}\hat{u}^2_{m,i+1/2}A. \quad (24)$$

The pressure gradient term is discretized using central differences:

$$\left(\frac{\partial p}{\partial s}\right)_i \approx [31]\frac{p_{i+1} - p_{i-1}}{s_{i+1} - s_{i-1}}, \quad (25)$$

while the gravitational source is evaluated as

$$(\rho_m g\cos\theta)_i = \rho_{m,i} g\cos\theta_i. \quad (26)$$

Friction is represented through a correlation of the form

$$f_{m,i} = \frac{1}{2}f_{\mathrm{fric},i}\frac{\rho_{m,i}u_{m,i}|u_{m,i}|}{D_{h,i}}A\Delta s_i, \quad (27)$$

where $f_{\mathrm{fric},i}$ is a friction factor, which may depend on Reynolds number, roughness, and flow regime.

Time integration is performed using an implicit or semi-implicit scheme to mitigate the severe stability restrictions that would arise from fully explicit methods, especially in the presence of high gas compressibility and stiff source terms. Letting [32] t^n denote the current time and $t^{n+1} = t^n + \Delta t^n$ the next time level, a first-order backward Euler method for a generic variable ϕ_i reads

$$\phi_i^{n+1} - \phi_i^n = \Delta t^n R_i\left(\phi^{n+1}\right), \quad (28)$$

where R_i is the discrete residual of the governing equation in cell i. Collecting all unknowns into a state vector [33] $\mathbf{x}^{n+1}$, the fully implicit time step requires the solution of a nonlinear system

$$\mathbf{F}\left(\mathbf{x}^{n+1}\right) = \mathbf{0}. \quad (29)$$

This system is solved using a Newton or modified Newton method. At each Newton iteration k, a linear system is assembled and solved,

$$\mathbf{J}\left(\mathbf{x}^{(k)}\right)\delta\mathbf{x}^{(k)} = -\mathbf{F}\left(\mathbf{x}^{(k)}\right), \quad (30)$$

where $\mathbf{J}$ is the Jacobian matrix of partial derivatives of the residuals with respect to the unknowns and $\delta\mathbf{x}^{(k)}$ is the update step. The new iterate is

$$\mathbf{x}^{(k+1)} = \mathbf{x}^{(k)} + \delta\mathbf{x}^{(k)}. \quad (31)$$

The Jacobian has a sparse banded structure corresponding to the one-dimensional grid coupling, and linear algebra solvers exploiting this structure are used to reduce computational cost. When a fully consistent Jacobian is expensive to assemble, approximate Jacobians or Jacobian-free methods can be employed with suitable preconditioners [34].

An alternative approach is to treat certain terms explicitly while keeping others implicit, leading to semi-implicit schemes. For example, convective terms can be discretized explicitly while pressure, compressibility, and stiff source terms are treated implicitly. This results in a linear system that is less nonlinear but still stable for practical time steps. The selection of terms to be treated implicitly is guided by linear stability analysis and numerical experimentation. For example, considering a linearized version of the mass and momentum equations around a steady state, one can derive a dispersion relation relating growth rate to wavenumber, from which a Courant–Friedrichs–Lewy type condition emerges. In explicit schemes, this leads to restrictions of the form

$$\Delta t^n [35] \le C_{\mathrm{CFL}} \min_i \frac{\Delta s_i}{|u_{m,i}| + c_{m,i}}, \quad (32)$$

where $c_{m,i}$ is an effective mixture wave speed and C_{CFL} is a stability constant less than unity. In implicit schemes, this restriction is significantly relaxed, enabling larger time steps that remain compatible with real-time or near real-time simulation requirements.

The solution of the discrete system yields pressure, mixture velocity, and phase fractions at each grid cell and time level. Gas and liquid velocities are reconstructed from the drift-flux relation. Thermodynamic quantities such as gas density and compressibility are updated using the local pressure and temperature. If thermal effects are included, an energy balance equation is discretized in an analogous finite volume framework, and temperature is evolved simultaneously [36]. The coupling between energy and mass–momentum equations can be handled within the same nonlinear system or via operator splitting, depending on the desired accuracy and computational cost.

Boundary conditions under variable pressure are incorporated directly into the discretized system. At the surface, the pressure in the first cell or at the upper interface is constrained by a choke model, which may

itself be a function of the predicted flow rate and a control action. For instance, a simple algebraic relation

$$Q_{\mathrm{surf}}^{n+1} = C_d u_c^{n+1} \sqrt{p_{\mathrm{well}}^{n+1} - p_{\mathrm{sep}}} \tag{33}$$

can be combined with the mass balance at the surface to enforce consistency between wellbore outflow, pressure, and choke opening. At the bottom, an influx model imposes a source term in the deepest cell based on the pressure difference between wellbore and formation, discretized consistently with the finite volume formulation [37]. Variable bottom-hole pressure programs, such as those associated with changes in pump rate or set-point in managed pressure drilling, are applied as time-varying constraints in the lower boundary conditions.

Overall, the numerical strategy combines finite volume discretization of the governing equations, implicit or semi-implicit time integration, and Newton-based nonlinear solvers with sparse linear algebra. This framework is flexible enough to accommodate different levels of model complexity, from simplified drift-flux approximations to more detailed two-fluid formulations, and to incorporate variable surface and bottom-hole pressure conditions representative of realistic drilling operations.

5 | Simulation of Gas Kick Scenarios under Variable Pressure Programs

The numerical framework is used to simulate gas kick scenarios in deviated and horizontal wells with varying pressure control strategies. Synthetic well trajectories are constructed by specifying the inclination angle $\theta(s)$ as a function of measured depth, including sections that transition from vertical to deviated and then to horizontal, as well as purely horizontal segments [38]. The annular geometry is defined by casing and drillstring diameters, and hydraulic parameters such as roughness and friction factor correlations are chosen to represent a typical drilling operation. Drilling fluid density, viscosity, and compressibility, along with gas properties, are specified according to representative field conditions.

Initial conditions consist of a fully liquid-filled annulus in steady circulation, with a given pump rate and surface pressure leading to a stable pressure profile along the well. The bottom-hole pressure is initially set to maintain a small overbalance with respect to the formation pressure. A gas influx is initiated by reducing the bottom-hole pressure below the formation pressure either through a transient change in pump rate, a reduction in surface backpressure, or a deliberate perturbation of fluid density. The influx model then introduces gas into the lowest cell according to the pressure difference, with the influx rate increasing as the underbalance grows and decreasing as wellbore pressure recovers.

One set of simulations investigates the evolution of a gas kick in a deviated well with variable surface pressure controlled by a manual choke operation [39]. The choke opening is modeled as a function of time, representing a sequence of manual adjustments aimed at maintaining bottom-hole pressure near a target value. During the early stages of the influx, the gas concentration in the lower part of the well increases, and the mixture density decreases, leading to a slower but steady rise in gas volume fraction in the inclined section. As the gas slug approaches the transition to a more vertical segment, its buoyant acceleration increases, and the local mixture velocity rises. This produces a noticeable signal in surface parameters, including an increase in flow-out relative to flow-in and a deviation in standpipe and casing pressures.

The simulation results show that gas migration and expansion in deviated sections may delay the onset of strong surface pressure signatures compared to a vertical well of similar depth and fluid properties. Gas may temporarily accumulate in near-horizontal sections, leading to spatially localized pockets of high gas fraction [40]. When these pockets encounter steeper segments of the trajectory, their buoyant rise is enhanced, and rapid pressure transients may occur. Variable surface pressure conditions interact with this behavior. For example, if the choke is adjusted to increase backpressure as a response to early indications of a kick, the imposed pressure change may compress the migrating gas, temporarily reducing its volume and moderating the hydrostatic loss. When the choke is subsequently opened to circulate the kick out, sudden expansion of compressed gas slugs can generate secondary pressure surges.

Another series of simulations examines managed pressure drilling strategies, in which surface pressure is regulated by an automatic choke control system to track a prescribed bottom-hole pressure set-point. The control law adjusts the choke opening based on deviations between measured and target bottom-hole pressure, typically using proportional–integral or more advanced control formulations. In the model, bottom-hole pressure is computed from the simulated pressure profile, and the control law is applied to update the choke opening at each time step [41]. Under such control, the bottom-hole pressure is kept

close to the target value during normal operations, and during the onset of a gas influx the system reacts by increasing surface backpressure. The simulations reveal that this approach can mitigate the growth of underbalance and reduce the total gas volume entering the wellbore, but it does not entirely eliminate the transient effects as the gas migrates and expands toward the surface.

In long horizontal wells, simulations indicate that the distribution of gas in the horizontal limb is sensitive to the interaction between buoyancy, friction, and imposed flow conditions. When pump rates are high and the horizontal section is relatively smooth, gas is more uniformly transported toward the heel, and flow regimes tend toward dispersed or churn flow. When pump rates are lower or when the well has local geometric irregularities, gas can segregate into large bubbles or slugs along the high side, with intermittent movement. These patterns translate into complex and sometimes intermittent surface responses [42]. For instance, the flow-out signal may exhibit oscillations as gas-rich slugs reach the surface, while pressure records show sequences of relatively quiet periods interrupted by sharp peaks. Under variable surface pressure conditions, these patterns may be further modulated, making interpretation based on surface data alone challenging.

Sensitivity studies within the simulation framework explore the effect of key parameters such as fluid density, gas compressibility, friction factor, and well inclination profile on the evolution of the kick. Reducing fluid density, for example, reduces the hydrostatic gradient and increases the sensitivity of bottom-hole pressure to frictional and dynamic effects. In such cases, small perturbations in pump rate or choke opening have a larger impact on the pressure profile and can more easily trigger an influx if not carefully controlled. Increasing gas compressibility, modeled through a higher compressibility factor or different gas composition, enhances the degree of expansion as gas migrates, leading to larger variations in mixture density and more pronounced transients. Changes in friction factor, representing variations in roughness or flow regime, alter the distribution of pressure losses along the well and thus the balance between hydrostatic and frictional contributions [43].

The simulations also provide spatial–temporal fields of gas volume fraction, velocity, and pressure that reveal internal mechanisms that are not directly observable in field measurements. For example, the movement of the leading and trailing edges of a gas slug can be tracked as it traverses different inclination zones, showing changes in shape and propagation speed. These detailed internal profiles form an important basis for understanding how different operational strategies influence the risk of secondary kicks, pressure surges, or unexpected gas arrivals at the surface. Furthermore, they serve as high-resolution synthetic data for training and validating data-driven models for kick detection and characterization, as discussed in the following section.

6 | Data-Driven Interpretation and Machine Learning Integration

The high-fidelity simulations of gas kick scenarios generate rich time series of surface and downhole variables, including pressures, flow rates, gas volume fractions, and phase velocities. These data can be used to construct machine-learning models aimed at early detection of gas kicks, estimation of influx size, and identification of risk-prone operating conditions [44]. The goal is not to replace physics-based modeling but to complement it by providing pattern recognition capabilities that are difficult to encode in explicit analytical rules, particularly in deviated and horizontal wells where transient signatures are complex.

To build such models, a set of simulation cases is generated by varying key parameters such as pump rate, choke control strategy, formation pressure, fluid density, and well trajectory. For each case, model outputs are sampled at a fixed time interval, producing sequences of surface measurements such as standpipe pressure $p_{\mathrm{sp}}(t)$, casing pressure $p_{\mathrm{csg}}(t)$, flow-in $Q_{\mathrm{in}}(t)$, flow-out $Q_{\mathrm{out}}(t)$, and pit volume $V_{\mathrm{pit}}(t)$. To represent the temporal dynamics, sliding time windows of length T_w are extracted, and each window is labeled according to the underlying physical state. For classification tasks, labels can represent categories such as normal operation, onset of kick, active kick circulation, and post-kick stabilization. For regression tasks, labels can be continuous-valued quantities such as cumulative influx volume, current gas fraction at a given depth, or predicted time to surface arrival [45].

The mapping from input time series to outputs is approximated using machine-learning architectures capable of capturing temporal dependencies.

Recurrent neural networks, including gated recurrent units or long short-term memory networks, can be applied by feeding sequences of measurement vectors $\mathbf{y}(t)$ and training the network to predict the associated labels. Alternatively, temporal convolutional networks can be employed to learn localized temporal patterns through one-dimensional convolutions along the time axis. Let $\mathbf{y}_k \in \mathbb{R}^m$ denote the vector of m

measurements at time step k in a window. A neural network model can be written abstractly as

$$\hat{\mathbf{z}} = \mathcal{M}\left([46]\mathbf{y}_1, \mathbf{y}_2, \ldots, \mathbf{y}_K; \boldsymbol{\theta}\right), \tag{34}$$

where $\hat{\mathbf{z}}$ is the predicted output (class probabilities or regression targets) and $\boldsymbol{\theta}$ denotes the model parameters. Training consists of minimizing a loss function

$$\mathcal{L}\left(\boldsymbol{\theta}\right) = \frac{1}{N_s} \sum_{n=1}^{N_s} \ell\left(\hat{\mathbf{z}}^{(n)}, \mathbf{z}^{(n)}\right), \tag{35}$$

where N_s is the number of training samples, [47] $\mathbf{z}^{(n)}$ are the true labels, and ℓ is a suitable loss, such as cross-entropy for classification or mean squared error for regression.

To quantify uncertainty and to incorporate probabilistic reasoning, Bayesian or probabilistic machine-learning approaches can be considered. For instance, a probabilistic classifier may output a probability $P(C_j \mid \mathbf{Y})$ for each class C_j given the time series $\mathbf{Y}$ in a window. In a simple parametric model, this can be expressed as

$$P(C_j \mid \mathbf{Y}) = \frac{\exp\left([48]\boldsymbol{\beta}_j^{\top} \boldsymbol{\phi}(\mathbf{Y})\right)}{\sum_l \exp\left(\boldsymbol{\beta}_l^{\top} \boldsymbol{\phi}(\mathbf{Y})\right)}, \tag{36}$$

where $\boldsymbol{\phi}(\mathbf{Y})$ is a feature vector extracted from the time series through, for example, summary statistics, wavelet coefficients, or principal component analysis, and $\boldsymbol{\beta}_j$ are model parameters. More flexible nonparametric techniques, including Gaussian processes or ensemble methods, can be applied when the dimensionality and complexity of the feature space permit.

The training and evaluation process leverages statistical validation methods to estimate generalization performance and to guard against overfitting to specific simulation cases. The available dataset is partitioned into training, validation, and test subsets [49]. During training, hyperparameters such as network depth, regularization strength, and learning rate are tuned based on validation performance. Metrics such as accuracy, precision, recall, and receiver operating characteristic curves are computed for classification tasks, while root mean squared error and other regression metrics are used for continuous outputs. The probabilistic nature of the predictions allows calibration analysis, whereby predicted probabilities are compared to empirical event frequencies to assess whether the model is well calibrated.

An important consideration in the use of simulation-based training data is the domain shift between synthetic and field conditions. The simulator depends on assumptions and parameter choices that may not fully reflect actual wells. To reduce this gap, parameter ranges for simulations can be chosen to cover plausible field variability in fluid properties, trajectory geometries, and operational practices. Furthermore, domain adaptation techniques can be applied when some labeled field data become available [50]. For example, transfer learning can be performed by taking a model trained on simulated data and fine-tuning its parameters using a smaller set of field cases. Alternatively, importance weighting methods can be used to adjust training loss contributions from different simulation scenarios so that the resulting model better reflects the distribution of field conditions.

Physical consistency is another critical aspect. Machine-learning models trained solely on data may violate basic physical constraints, such as conservation of mass or monotonic relationships between key variables. To mitigate this, physics-informed machine-learning strategies embed constraints derived from the governing equations or from expert knowledge. For instance, features can be constructed to enforce mass balance relationships between flow-in, flow-out, and pit volume changes, and the model can be penalized when its predictions imply unphysical violations of these relationships [51]. In more advanced settings, the loss function includes terms that measure deviations from approximate solutions of simplified physical models, thereby encouraging the learned mapping to respect known physical trends.

Linear algebra and tensor calculations are heavily used in implementing and training these models. For example, the feature matrices for all time windows can be assembled into a tensor $\mathcal{Y} \in \mathbb{R}^{N_s \times K \times m}$, and training involves repeated multiplication of this tensor with weight matrices in the neural network layers. Optimization of the model parameters proceeds by gradient-based methods such as stochastic gradient descent or its variants, which rely on backpropagation through the computational graph. The gradients are computed using automatic differentiation and can be interpreted as the product of Jacobian matrices of layer transformations. In some cases, regularization terms of the form

$$R(\boldsymbol{\theta}) = \lambda[52]\|\boldsymbol{\theta}\|_2^2 \tag{37}$$

are added to the loss, where λ is a regularization coefficient and $\|\cdot\|_2$ denotes the Euclidean norm, to control the complexity of the model and improve

generalization.
The integrated framework thus couples detailed physics-based simulations of gas kick behavior in deviated and horizontal wells with machine-learning models for interpretation of surface measurements. The physical model provides high-resolution, labeled data capturing the diversity of kick manifestations under different pressure control strategies and well configurations. The data-driven model, in turn, offers a compact representation of the mapping from observed signals to underlying states and quantities of interest, which can support decision making in real time [53]. The interplay between these components is further examined in the discussion section.

7 | Discussion

The combined modeling and simulation framework developed for gas kick behavior in deviated and horizontal wellbores under variable pressure conditions highlights the complexity of transient multiphase flow and the subtleties of interpreting surface measurements. The physical model reveals that inclination plays an essential role not only in modifying the hydrostatic contribution to pressure but also in shaping the flow regimes and migration patterns of gas during a kick. In horizontal sections, stratification and segregation effects lead to localized pockets of gas that may attenuate or delay the surface manifestation of an influx. This behavior contrasts with vertical wells, where gas tends to migrate more uniformly upward, producing relatively clearer and earlier surface signatures.
Variable pressure boundary conditions, such as those imposed by manual choke operations or automated managed pressure drilling systems, add another layer of complexity. Their interactions with gas migration can both mitigate and complicate kick behavior [54]. For example, rapidly increasing surface backpressure can reduce the effective underbalance at the bottom and thus limit further influx, but it can also compress existing gas slugs and delay their expansion until the choke is opened. The simulations show that such sequences of compression and expansion may lead to non-intuitive pressure transients and highlight the importance of considering the full space–time evolution of gas within the wellbore when designing and evaluating control strategies.
From a numerical perspective, the governing equations constitute a stiff, nonlinear system that requires careful discretization and robust solution methods. Finite volume schemes ensure discrete conservation, which is crucial for accurately tracking gas volumes during kicks. Implicit or semi-implicit time stepping relieves the stringent stability constraints associated with high gas compressibility and strong coupling between pressure and density. Newton-based nonlinear solvers with appropriate preconditioning are necessary to converge reliably, particularly when steep gradients, sharp interfaces, or strong boundary condition changes arise [55]. The linear algebraic structure of the discretized system, with its banded or block-banded sparsity, can be exploited to improve computational efficiency in practical implementations.
The integration of machine-learning models into the framework offers a mechanism to translate complex simulation outputs into operationally usable information. By training on a broad ensemble of simulated scenarios, data-driven models learn to associate surface measurement patterns with gas kick states and parameters. However, the study also underscores several limitations and challenges. One is the representativeness of simulation-based training data. Even though simulations can cover a wide range of conditions, they are constrained by modeling assumptions and parameterizations. If the actual field behavior deviates significantly from the model, the machine-learning tools may exhibit degraded performance when deployed [56]. This suggests a need for continuous updating and calibration of the models as field data become available.
Another challenge lies in the tension between model complexity and interpretability. Deep architectures can capture intricate temporal patterns in measurement data, but their internal representations may be difficult to interpret in terms of physical mechanisms. For critical decision-making tasks like well control, operators often prefer tools that provide not only predictions but also insight into why a kick is suspected and how confident the tool is. Methods for explaining model predictions, such as sensitivity analysis or feature attribution, can help bridge this gap. In addition, incorporating physical constraints and prior knowledge into the machine-learning model, for example through physics-informed architectures or constrained loss functions, can improve both predictive reliability and interpretability [57].
Statistical validation and uncertainty quantification are essential when evaluating the potential operational value of data-driven models. The probabilistic outputs of classifiers and regressors should be assessed for calibration and robustness to variations in input conditions, including noise, missing data, and sensor failures. Simulation studies can introduce such perturbations in a controlled manner, allowing the investigation of how model performance degrades

under degraded data quality. This is particularly relevant in deviated and horizontal wells, where sensor placement and reliability may be more constrained than in vertical wells, and where certain measurements, such as downhole pressures, might not always be available.

Finally, the interaction between model predictions and control strategies warrants attention. If machine-learning outputs are used to trigger automatic responses in choke settings, pump rates, or other control actions, feedback loops are created between the predictive tool and the physical system. These feedbacks can potentially amplify modeling errors or biases if not properly accounted for [58]. One approach is to test such closed-loop strategies in the simulation framework, treating the data-driven models as components within the control loop and examining the resulting system behavior across many scenarios. This can reveal conditions under which the combined system behaves robustly and conditions under which it may become unstable or overly conservative.

Overall, the discussion highlights that modeling and simulation of gas kicks in deviated and horizontal wells, coupled with data-driven interpretation, provide a structured way to analyze and understand complex well control phenomena. At the same time, careful consideration of modeling assumptions, numerical methods, statistical validation, and operational integration is necessary to use such tools responsibly and effectively.

8 | Conclusion

A comprehensive framework for modeling and simulation of gas kick behavior in deviated and horizontal wellbores under variable pressure conditions has been presented, combining transient multiphase flow modeling with numerical methods and data-driven interpretation. The physical model, formulated along the well trajectory, accounts for inclination-dependent gravity, compressible gas behavior, and time-varying boundary pressures arising from choke operations and managed pressure drilling strategies [59]. Through finite volume discretization and implicit or semi-implicit time integration, the stiff nonlinear system of governing equations is solved to obtain the spatial–temporal evolution of pressure, velocities, and phase fractions during kick scenarios.

The simulations illustrate how wellbore inclination and horizontal sections modify gas migration and expansion patterns compared to vertical wells. Stratification and high-side gas accumulation in horizontal intervals can delay and distort surface signatures, while transitions to more vertical segments can trigger rapid gas acceleration and pronounced pressure transients. Variable surface pressure programs interact strongly with these dynamics, influencing both the amount of gas influx and the subsequent evolution of gas slugs as they move toward the surface. Sensitivity analyses show that fluid properties, friction, and trajectory geometry all have a significant impact on the magnitude and timing of observed responses during a gas kick.

On the data-driven side, synthetic simulation outputs provide labeled time series for training machine-learning models aimed at kick detection and characterization based on surface measurements. Recurrent and convolutional neural network architectures, along with probabilistic models, can learn mappings from measurement histories to underlying states such as onset of kick, influx volume, and risk indicators [60]. Statistical validation highlights the importance of robust training practices, uncertainty quantification, and calibration, especially when models are to be used in operational settings. Physics-informed strategies and domain adaptation techniques offer pathways for improving the transfer of such models from synthetic to field environments.

The integrated viewpoint adopted here underscores the complementary roles of physics-based and data-driven methods. Detailed multiphase flow simulations provide insight into mechanisms and furnish structured data, while machine-learning models condense complex patterns into operationally useful predictions. Limitations remain, including uncertainties in model parameters, possible discrepancies between simulated and actual behavior, and challenges in ensuring reliable performance under varying conditions and data quality. Future work may focus on extending the physical model to include more detailed thermal and three-dimensional effects, enhancing the statistical treatment of uncertainty, and incorporating field data to refine and validate both the simulations and the machine-learning models. In this way, the framework can evolve to support more informed and responsive well control strategies in deviated and horizontal drilling environments under variable pressure conditions [61].

References

[1] F. W. Ng, “Removal of water base mud from well bores in permafrost zones,” *Journal of Engineering for Industry*, vol. 98, pp. 701–707, 5 1976.

[2] J. Jiang, F. Rabbi, and Q. Wang, "Underbalanced drilling technology with air injection connector," *Journal of Petroleum Exploration and Production Technology*, vol. 4, pp. 275–280, 11 2013.

[3] S. Leach, G. M. Smith, and R. G. Berndt, "Sme special session: Subsea slurry lift pump technology - sms development," in *Offshore Technology Conference*, OTC, 4 2012.

[4] J. Åge Stakvik, C. Berg, G.-O. Kaasa, O. M. Aamo, and U. Lehner, "Adaptive model based choke control system for mpd operations," in *SPE/IADC Managed Pressure Drilling and Underbalanced Operations Conference and Exhibition*, SPE, 4 2016.

[5] X. J. Zhang, S. Taoutaou, Y. Guo, Y. L. An, S. M. Zhong, and Y. Wang, "Engineering cementing solution for hutubi underground gas storage project," in *SPE Unconventional Gas Conference and Exhibition*, SPE, 1 2013.

[6] K. Witwer, "Test report for core drilling ignitability testing," 8 1996.

[7] V. O. Yablonskii, "Modeling of degassing of viscoplastic liquids in a cylindrical hydrocyclone," *Russian Journal of Applied Chemistry*, vol. 95, pp. 270–276, 6 2022.

[8] K. Manikonda, A. R. Hasan, O. Kaldirim, J. J. Schubert, and M. A. Rahman, "Understanding gas kick behavior in water and oil-based drilling fluids," in *SPE Kuwait oil and gas show and conference*, p. D043S023R001, SPE, 2019.

[9] Q. You, G. Zhao, and X. Sun, *Gels for Oil and Gas Industry Applications*. MDPI, 8 2022.

[10] W. Chen, "Status and challenges of chinese deepwater oil and gas development," *Petroleum Science*, vol. 8, pp. 477–484, 12 2011.

[11] M. W. Massey, "Marine well containment company progress," in *Offshore Technology Conference*, OTC, 4 2012.

[12] S. Bertram-Howery and P. Swift, "Potential for long-term isolation by the waste isolation pilot plant disposal system," 6 1990.

[13] R. Akhmiyeva, "Influence of the oil industry on anthropogenic changes in natural landscapes," *SHS Web of Conferences*, vol. 128, pp. 3003–03003, 12 2021.

[14] "Oil and gas r&d programs," 3 1997.

[15] D. Dean, "Bodcau in situ combustion project. final report, june 1976-june 1982," 12 1982.

[16] R. Stork, "Computer model simplifies gas field production forecasting and development planning," *The APPEA Journal*, vol. 27, pp. 335–343, 6 1987.

[17] E. Chiuzan, R. Dragoescu, N. Ianc, A. Matei, and A. Camarasescu, "Methane emissions from the mines belonging to the hunedoara energy complex," *MATEC Web of Conferences*, vol. 354, pp. 25–00025, 1 2022.

[18] M. Khodja, M. Khodja-Saber, J. P. Canselier, N. Cohaut, and F. Bergaya, *Drilling Fluid Technology: Performances and Environmental Considerations*. Sciyo, 11 2010.

[19] P. H. Lampén and A. Nikula, "Groundwater investigations in the lavia deep drilling hole-sampling techniques and results," *Water Science and Technology*, vol. 20, pp. 223–224, 3 1988.

[20] D. Ermak, "Potential growth of electric power production from imperial valley geothermal resources," 9 1977.

[21] C. Gruber, H. F. Spoerker, and W. Brandstaetter, "Dynamic modeling of gas distribution in the wellbore during kick situations: The solutions," *IADC/SPE Drilling Conference and Exhibition*, 3 2014.

[22] A. C. Lage, E. Nakagawa, R. W. Time, E. H. Vefring, and R. Rommetveit, "Full-scale experimental study for improved understanding of transient phenomena in underbalanced drilling operations," *SPE/IADC Drilling Conference*, 3 1999.

[23] "Petroleum: An energy profile, 1999," 7 1999.

[24] N. G. Author, "Project rio blanco definition plan. additional formation evaluation and production testing," 9 1975.

[25] S. Vij, S. Narasaiah, A. Walia, and G. Singh, "Multilaterals: An overview and issues involved in adopting this technology," in *SPE India Oil and Gas Conference and Exhibition*, SPE, 2 1998.

[26] N. St.Michel, J. J. Xu, J. Harrist, G. D. Zhan, and A. Aljohar, "Automated fluid rheology measurement at the drillsite," in *ADIPEC*, SPE, 10 2022.

[27] M. R. Darwish, M. Nabucet, J. Cabillic, Y. Metwalli, and Y. El-Khazindar, "Optimize drilling costs and improving safety, environment and operational performance by utilizing a barge, an abu dhabi experience," in *Abu Dhabi International Petroleum Exhibition and Conference*, SPE, 10 2002.

[28] L. Gao, X. Kang, M. Tang, J. Hu, J. Ren, and C. Zhou, "Study on prediction of outburst risk of excavation face by initial gas emission," *Geofluids*, vol. 2022, pp. 1–9, 3 2022.

[29] T. Huszar, G. Wittenberger, and E. Skvarekova, "Warning signs of high-pressure formations of abnormal contour pressures when drilling for oil and natural gas," *Processes*, vol. 10, pp. 1106–1106, 6 2022.

[30] G. R. Darmawan, N. B. Sangka, S. D. Susilo, J. T. Shaun, S. W. Nas, A. E. Prasetia, and S. Sisworo, "Integrated downhole isolation valve and managed pressure drilling to facilitate development of sour fractured-limestone gas reservoir in east java, indonesia," *SPE/IADC Drilling Conference and Exhibition*, 3 2011.

[31] K. Manikonda, A. R. Hasan, A. Barooah, N. H. Rahmani, M. El-Naas, A. K. Sleiti, and M. A. Rahman, "A mechanistic gas kick model to simulate gas in a riser with water and synthetic-based drilling fluid," in *Abu Dhabi International Petroleum Exhibition and Conference*, p. D012S116R009, SPE, 2020.

[32] J. Labaj and D. Barta, "Unsteady flow simulation and combustion of ethanol in diesel engines," *Communications - Scientific letters of the University of Zilina*, vol. 8, pp. 27–37, 6 2006.

[33] F. Huszarik, J. Reichman, and C. Jb, "Use of high-pressure waterjets in utility industry applications," *Erosion: Prevention and Useful Applications*, pp. 597–615, 1 1979.

[34] L. Brown and A. Vadie, "The utilization of the microflora indigenous to and present in oil-bearing formations to selectively plug the more porous zones thereby increasing oil recovery during waterflooding. annual report for the period, january 1, 1994–december 31, 1994," 8 1995.

[35] R. Lee, R. B. Grigg, and B. McPherson, "Validation and comparison of carbon sequestration project cost models with project cost data obtained from the southwest partnership," 4 2011.

[36] C. M. Oldenburg, "Health, safety, and environmental risks from energy production: A year-long reality check," *Greenhouse Gases: Science and Technology*, vol. 1, pp. 102–104, 5 2011.

[37] T. Bartke, D. Fischer, S. King, R. Boyd, and A. Humphrey, "Hanna, wyoming underground coal gasification data base. volume 3. the hanna ii, phase i field test," 8 1985.

[38] M. Hernandez, D. W. MacNeill, M. Reeves, A. D. Kirkwood, J. Ruszka, R. Zaeper, and S. R. Lemke, "High-speed wired drillstring telemetry network delivers increased safety, efficiency, reliability, and productivity to the drilling industry," in *SPE Indian Oil and Gas Technical Conference and Exhibition*, SPE, 3 2008.

[39] A. Al-Mutairi, H. A. Baqer, A. K. Dhabria, G.-J. Rook, A. K. Shaik, B. Al-Mutairi, K.-K. Hii, and A. A. Hadi, "Successful installation of 1st 15k multistage completion system in north kuwait gas well," in *SPE Kuwait Oil & Gas Show and Conference*, SPE, 10 2017.

[40] L. Pasimeni, I. Lukman, B. Tlepbergenov, A. Dadinov, T. Kabbasov, Y. Yeskairov, D. Zhumashev, A. Suleimenov, A. Aliyeva, A. Zholdaskaliyev, A. S. Z. Ariff, and O. M. Okorie, "Rfid technology expanded into the drilling space with particular emphasis on efficiencies," in *Day 2 Thu, October 22, 2020*, SPE, 10 2020.

[41] A. Zankawi, "Modeling gas migration during a gas kick," 1 2021.

[42] "Record of decision for amchitka surface closure, alaska," 8 2008.

[43] H. Woith, J. Vlček, T. Vylita, T. Dahm, T. Fischer, K. Daskalopoulou, M. Zimmer, S. Niedermann, J. A. Stammeier, V. Turjaková, and M. Lanzendörfer, "Effect of pressure perturbations on co2 degassing in a mofette system: The case of hartoušov, czech republic," *Geosciences*, vol. 13, pp. 2–2, 12 2022.

[44] H. Shi, G. Li, Z. Huang, and S. Shi, "Properties and testing of a hydraulic pulse jet and its application in offshore drilling," *Petroleum Science*, vol. 11, pp. 401–407, 7 2014.

[45] "[environmental investigation of ground water contamination at wright-patterson air force base, ohio]. volume 3, appendix a, draft standard

operating procedures and elements: Sampling and analysis plan (sap): Phase 1, task 4, field investigation, draft," 10 1991.

[46] M. Tajuddin, A. W. A. Tajuddin, M. Z. Aznor, P. Harbidge, and J. Chanson, "New method to reduce drilling survey time, cost and risk for wells drilled offshore malaysia," in *Offshore Technology Conference Asia*, OTC, 3 2016.

[47] "Eia model documentation: Documentation of the oil and gas supply module (ogsm)," 1 1997.

[48] A. Mahmood, L. Ring, A. Alajbegovic, and S. Nienhuis, "Enabling new techniques: Nitrogen gas qualification and testing of a rotating control device," in *IADC/SPE Managed Pressure Drilling & Underbalanced Operations Conference & Exhibition*, SPE, 3 2017.

[49] W. Maurer and G. Medley, "Development and testing of underbalanced drilling products," 7 1995.

[50] K. Theimer and J. J. Kolle, "Microhole high-pressure jet drill for coiled tubing," 6 2007.

[51] F. Xiao, Z. Zhao, and L. Yang, "Innovative measures for thermal performance enhancement of single well-based deep geothermal systems: existing solutions and some viable options," *Geomechanics and Geophysics for Geo-Energy and Geo-Resources*, vol. 8, 7 2022.

[52] M. Yamamoto, M. Murai, K. Maeda, and S. Uto, "An experimental study of the interaction between pipe structure and internal flow," in *Volume 3: Pipeline and Riser Technology*, pp. 213–220, ASMEDC, 1 2009.

[53] A. Kamel, "A technical review of radial jet drilling," *Journal of Petroleum and Gas Engineering*, vol. 8, pp. 79–89, 10 2017.

[54] C. R. Johnson, S. Sari, A. Ahrenst, and I. Gozubuyuk, "Energy transition by employing a self-healing, reduced carbon dioxide footprint sealant in a strategic underground gas storage project," in *SPE EuropEC - Europe Energy Conference featured at the 83rd EAGE Annual Conference & Exhibition*, SPE, 6 2022.

[55] L. Kumar, M. S. Hossain, M. E. H. Assad, and M. U. Manoo, "Technological advancements and challenges of geothermal energy systems: A comprehensive review," *Energies*, vol. 15, pp. 9058–9058, 11 2022.

[56] C. Goranson, "Applicability of petroleum horizontal drilling technology to hazardous waste site characterization and remediation," 9 1992.

[57] A. Matei and N. Ianc, "Classification of underground mining works within the tg. ocna salt mine from the point of view of gas emissions," *MATEC Web of Conferences*, vol. 354, pp. 28–00028, 1 2022.

[58] K. Manikonda, A. R. Hasan, O. Kaldirim, N. Rahmani, and M. A. Rahman, "Estimating swelling in oil-based mud due to gas kick dissolution," in *International conference on offshore mechanics and arctic engineering*, vol. 84430, p. V011T11A039, American Society of Mechanical Engineers, 2020.

[59] M. C. Halim, H. Hamidi, and A. R. Akisanya, "Minimizing formation damage in drilling operations: A critical point for optimizing productivity in sandstone reservoirs intercalated with clay," *Energies*, vol. 15, pp. 162–162, 12 2021.

[60] J. S. S. Toralde, "Technology update: Retrofitting mpd systems to deepwater rigs aids drilling, efficiency, and process safety," *Journal of Petroleum Technology*, vol. 69, pp. 20–21, 2 2017.

[61] "Corrective action investigation plan for corrective action unit 527: Horn silver mine, nevada test site, nevada: Revision 1 (including records of technical change no.1, 2, 3, and 4)," 12 2002.